Alternative pathways for the development of lymphoid structures in humans

Laureline Berteloot[a,b,1], Thierry Jo Molina[c,d,1], Julie Bruneau[c,d], Capucine Picard[c,e,f], Vincent Barlogis[g], Véronique Secq[h,i,j,k], Chrystelle Abdo[l], Nathalie Boddaert[a,b,c], Claude Griscelli[b,m], Bénédicte Neven[b,c,f,m], and Alain Fischer[b,m,n,2]

[a]Department of Pediatric Radiology, Assistance Publique des Hopitaux de Paris, Necker Hospital for Sick Children, 75015 Paris, France; [b]INSERM UMR 1163, Institut Imagine, 75015 Paris, France; [c]University of Paris, 75015 Paris, France; [d]Department of Pathology, Assistance Publique des Hôpitaux de Paris, Hospital Robert Debré, Necker Hospital for Sick Children, 75015 Paris, France; [e]Study Center for Primary Immunodeficiencies, Necker Hospital for Sick Children, Assistance Publique des Hôpitaux de Paris, University of Paris, 75015 Paris, France; [f]Laboratory of Lymphocyte Activation and Susceptibility to EBV, INSERM UMR1163, Imagine Institute, Paris University, 75015 Paris, France; [g]Pediatric Hematology Department, Assistance Publique des Hopitaux de Marseille, Timone Enfant Hospital, 13005 Marseille, France; [h]Centre de Recherche en Cancérologie de Marseille, Unité 1068, INSERM, 13009 Marseille, France; [i]Institut Paoli-Calmettes, 13009 Marseille, France; [j]UMR 7258, CNRS, 13009 Marseille, France; [k]Université Aix-Marseille, 13007 Marseille, France; [l]Department of Hematology, Assistance Publique des Hopitaux de Paris, Necker Hospital for Sick Children, 75015 Paris, France; [m]Pediatric Hematology and Immunology Unit, Assistance Publique des Hopitaux de Marseille, Necker Hospital for Sick Children, 75015 Paris, France; and [n]Collège de France, 75231 Paris, France

Contributed by Alain Fischer, June 8, 2021 (sent for review May 4, 2021; reviewed by Thomas Boehm and Martin F. Flajnik)

Lymphoid tissue inducer (LTi) cells are critical for inducing the differentiation of most secondary lymphoid organs (SLOs) in mice. In humans, JAK3 and γc deficiencies result in severe combined immunodeficiency (SCIDs) characterized by an absence of T cells, natural killer cells, innate lymphoid cells (ILCs), and presumably LTi cells. Some of these patients have undergone allogeneic stem cell transplantation (HSCT) in the absence of myeloablation, which leads to donor T cell engraftment, while other leukocyte subsets are of host origin. By using MRI to look for SLOs in nine of these patients 16 to 44 y after HSCT, we discovered that SLOs were exclusively found in the three areas of the abdomen that drain the intestinal tract. A postmortem examination of a child with γc-SCID who had died 3.5 mo after HSCT showed corticomedullary differentiation in the thymus, T cell zones in the spleen, and the appendix, but in neither lymph nodes nor Peyer patches. Tertiary lymphoid organs were observed in the lung. No RAR-related orphan receptor-positive LTi cells could be detected in the existing lymphoid structures. These results suggest that while LTi cells are required for the genesis of most SLOs in humans, SLO in the appendix and in gut-draining areas, as well as tertiary lymphoid organs, can be generated likely by LTi cell-independent mechanisms.

lymphoid tissue | immune system | lymphoid organs

Lymphoid organogenesis in mammals is organized into three chronologically and mechanistically distinct steps: 1) the genesis of primary lymphoid organs, such as the thymus and the bone marrow; 2) the development of secondary lymphoid organs (SLOs), including lymph nodes, Peyer patches, and the spleen; and 3) the formation of tertiary lymphoid organs (TLOs) within tissues after the initiation of an immune response (1–3). In mice, lymphoid tissue-inducer (LTi) cells, a cell subset of hematopoietic origin that is related to the natural killer (NK)-innate lymphoid cell (ILC) lineage, orchestrate the generation of most SLOs with the exception of the splenic white pulp (4–8). The differentiation of LTi cells is dependent on an interleukin (IL)-7 signal, since IL-7 receptor knockout mice are devoid of LTi cells and most of the SLOs (4–7, 9–12).

Little is known about lymphoid organogenesis in humans. LTi-like cells (i.e., cells expressing molecules, such as the RAR-related orphan receptor C [RORC], lymphotoxin, and RANK ligand) have been detected in several sets of lymphoid structures (13–16). In humans, a hereditary lack of molecules required for LTi cell development (e.g., γc, JAK3, and IL-7Rα) causes severe combined immunodeficiency (SCID) and thus the absence of T cells, NK lymphocytes, and ILCs to which LTi cells are related (17–22). One can reasonably presume that these patients also lack LTi cells. Indeed, the patients with SCID caused by γc or JAK3 deficiency do not have detectable peripheral lymph nodes, in contrast to SCID caused by RAG-1 deficiency, in which only T and B cell development is impaired (23).

In order to provide these patients with an adaptive immune system, allogeneic hematopoietic stem cell transplantation (HSCT) can be performed after limited myeloablative chemotherapy or even in the absence of conditioning (18, 24–26). In many cases, the HSCT results in split chimerism that can persist for decades: that is, the T cells are of donor origin but all other blood lineages (including B cells and myeloid cells) are of host origin (18, 27). We have reported previously that these SCID patients also lack NK cells and ILCs long after HSCT (19). Taken as a whole, these data indicate that long-lived donor T cells and, perhaps, residual thymopoiesis persist in the absence of long-term donor stem cell engraftment (18). We took advantage of this unique setting to investigate the development of lymphoid structures. Hence, we used MRI to visualize SLOs in nine patients (P1 to P9) with SCID due to γc, JAK3, or IL-7Rα deficiency 16 to 44 y after HSCT. We also

Significance

Development of secondary lymphoid organs (SLO) was shown in mice to depend on lymphoid tissue inducer cells (LTi). Mutations of the IL2RG/JAK3 genes lead to severe combined immunodeficiency (SCID) characterized by an absence of T cells, natural killer cells, innate lymphoid cells, and likely LTi lymphocytes. Development of SLO was evaluated in T cell–reconstituted SCID patients by MRI, showing that lymph nodes were not detectable with the exception of those draining the gut. Analysis of tissues from a patient who died despite T cell reconstitution showed that lymph nodes were absent and that no LTi cells could be seen in the lymphoid-rich spleen and appendix. Thus, a LTi-independent pathway, mostly associated with the gut, contributes to SLO formation.

Author contributions: B.N. and A.F. designed research; L.B., T.J.M., J.B., C.P., C.A., N.B., and B.N. performed research; L.B., T.J.M., J.B., C.P., N.B., C.G., and A.F. analyzed data; V.B. provided clinical and immunological information on patient 11; C.P. performed blood immunophenotyping; C.A. performed TCR repertoire analysis; V.S. performed the immunohistology analysis of samples from patient 11; C.G. provided patient care (patient 10); and L.B., T.J.M., and A.F. wrote the paper.

Reviewers: T.B., Max Planck Institute of Immunobiology and Epigenetics; and M.F.F., University of Maryland, Baltimore.

The authors declare no competing interest.

[1]L.B. and T.J.M. contributed equally to this work.

[2]To whom correspondence may be addressed. Email: alain.fischer@aphp.fr.

This article contains supporting information online at https://www.pnas.org/lookup/suppl/doi:10.1073/pnas.2108082118/-/DCSupplemental.

Published July 14, 2021.

analyzed tissue samples from two other patients (P10, P11) having undergone HSCT, one who had died and another who had additionally received a lung transplant.

Results

Peripheral SLOs in SCID-IL2RG/JAK3/IL-7Rα Transplanted Patients. P1 to P9 were in good general health and had reconstituted a functional peripheral T cell pool, but none had detectable peripheral lymph nodes in cervical axillary, crural, and inguinal areas during repeated clinical examinations over a follow-up period of up to 44 y (median 29 y) (Table 1). Similarly, no tonsils were detectable (see *SI Appendix*, Fig. S1 for an illustrative example for P6). At the age of 31, P11 did not have any detectable tonsils or peripheral lymph nodes.

MRI Analysis of Lymphoid Organs in SCID Patients. The nine patients (median age 28 y) and nine controls (median age 32 y) underwent MRI. One control underwent MRI of the thorax only. Lymph nodes were found in 22 of the 152 examined sites (14%) in patients and 103 of the 140 examined sites (74%) in controls ($P < 0.001$). The median (range) number of sites with lymph nodes was 3 (0 to 4) per patient (56 nodes in total) in SCID patients and 13 (6 to 15) per control (467 nodes in total) (Figs. 1 and 2 and Table 2). Lymph nodes in peripheral (axillary and femoral) areas were found in none of the patients and all of the controls. Lymph nodes in the thorax were found in only two patients (one each), whereas they were found in all controls (in one to six thoracic areas each). In the abdominopelvic region, lymph nodes were identified in two (0 to 4) areas in patients and in seven (6 to 9) in controls. Remarkably, the lymph nodes detected in patients were always located in the same three sites (i.e., coeliomesenteric, interaortocaval, and paraaortic) (Table 2). The mean long axis of the major lymph nodes identified in each of these areas was significantly greater in patients than in controls (16 mm and 9.8 mm, respectively; $P = 9.8 \times 10^{-8}$ Student's *t* test). In patients, the lymph nodes were often grouped into small clusters within a limited area (Fig. 2 *A*–*C* and *SI Appendix*, Fig. S3).

Detection of a Typical Thymus but a Profound Lack of SLO in Postmortem Examination of P10. A thymus (weight: 7.5 g) was found in the postmortem examination of P10 3.5 mo after HSCT. This patient had evidence of T cell reconstitution (*Materials and Methods*) and died from brain sequelae of *Listeria* infection. Immunohistology revealed a clear-cut cortex-medulla differentiation and the presence of $CD3^+$ T cells (indicating active thymopoiesis), which differed distinctly from the abnormal thymus in SCID (28), thus attesting that T cell development was initiated by HSCT (Fig. 3 *A* and *B*). In contrast, no lymph nodes were detected macroscopically in peripheral areas (axillary and femoral) or mediastinal, mesenteric, or retroperitoneal areas. No tonsils were present. The only exception was a small parapancreatic lymph node with detectable T and B cells found on a pancreatic tissue section. Although the spleen was small (weight: ~15 g), it had a normal architecture, including regularly distributed white and red pulp with B cell follicles and

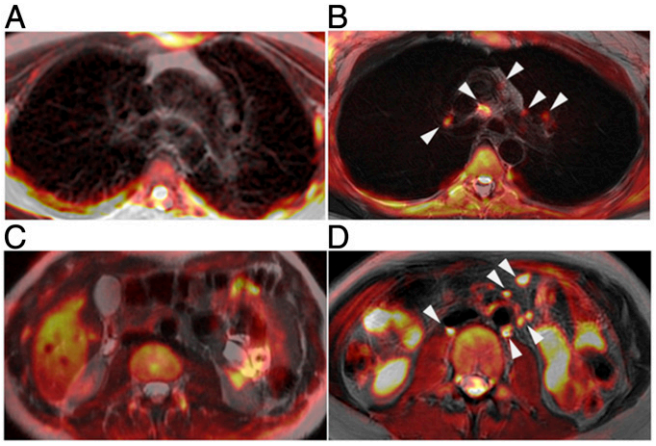

Fig. 1. MRI shows that transplanted SCID patients have few lymph nodes. Merged T2-weighted and DWI datasets. In a 25-y-old female patient (P7, *Left*), no lymph-node-like structures were visible in the thorax (*A*) or the abdomen (*C*). In a 31 y-old control (*Right*), several lymph node structures are visible in the hilar, mediastinal (*B*), intraperitoneal, and retroperitoneal areas (*D*) (arrowheads).

Table 1. Characteristics of transplanted SCID patients who underwent MRI examination

	Control	P1	P2	P3	P4	P5	P6	P7	P8	P9
Age (y)/gender		44/M	38/M	37/F	33/M	29/M	27/M	25/F	18/M	16/M
Molecular diagnosis		IL2RG	JAK3	JAK3	IL7R	IL2RG	IL2RG	JAK3	IL2RG	IL2RG
HSCT donor		Pheno-id	Haplo-id	Haplo-id	Haplo-id	Haplo-id	Haplo-id	Haplo-id	Haplo-id	Haplo-id
CR		No CR	bu8-cy	No CR	bu8-cy	No CR	bu8-cy	No CR	No CR	No CR
Clinical status		A.W.	chronic HPV	A.W	chronic HPV	A.W	A.W.	A.W	A.W.	chronic HPV
Chimerism T cells (D, %)		>99	>99	>99	>99	>99	>99	>99	>99	>99
B Cells (D, %)		1	ND	9	< 1	ND	< 1	ND	ND	< 10
Monocytes (D, %)		<1	< 1	2	< 1	< 1	< 1	< 1	< 1	< 10
IgG substitution		Y	N	Y	N	N	N	N	Y	Y
Age at last immunophenotype	(y)	44	37	37	33	28	27	25	18	16
CD3 (/μL)	807–1,844	996	1,689	1,064	578	1,564	399	840	740	681
CD4 (/μL)	460–1,232	273	691	233	455	471	175	287	209	144
CD8 (/μL)	187–844	696	**902**	820	124	**1,026**	180	471	461	537
Naive CD4 (/μL)	150–550	11	69	12	32	90	3.5	46	4	7
Naive CD8 (/μL)	60–270	0	**369**	8	9	**379**	24	122	28	38
Central memory (/μL)	oct-80	10	**441**	**115**	4	**380**	47	**330**	28	0
Effector memory (/μL)	80–220	**580**	27	**524**	100	41	59	14	189	**520**
TEMRA (/μL)	30–200	108	63	172	12	**225**	49	5	216	10
CD19 (/μL)	150–255	**355**	**219**	22	**155**	101	63	**174**	113	53
CD16-CD56 (/μL)	89–362	14	19	22	300	8	24	10	17	23

Underlined, lower than normal; bold, higher than normal; AW, alive and well; Bu, Busulfan; CR, conditioning regimen; Cy, cyclophosphamide; D, donor, F, female; Haplo-id, haploidentical donor; HPV, human papilloma virus infection; HSCT, hematopoietic stem cell transplantation; M, male; N, no; ND, not done; Pheno-id, phenoidentical donor; Y, yes. Patients with HPV infection were otherwise doing well; naive T CD4: $CD45RA^+$ $CD3^+$; naive T CD8: $CCR7^+$, $CD45RA^+$; central memory: $CCR7^+$, $CD45RA^-$; effector memory: $CCR7^-$ $CD45RA^-$; TEMRA: $CCR7^-$ $CD45RA^+$.

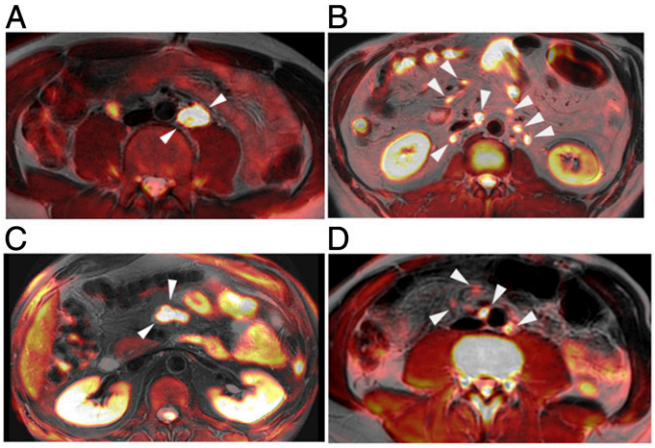

Fig. 2. MRI detects lymph nodes in some areas of the abdomen in transplanted SCID patients. Fusion imaging of T2-weighted sequences and DWI in male patient (P6) (*A* and *C*) and controls (*B* and *D*). Some large isolated lymph formations are visualized in the retroperitoneal region and in the celio-mesenteric areas in a 27-y-old patient (P6) and a 44-y-old (*C*, arrowheads) (P1), respectively. In controls, lymph nodes are more numerous and smaller-sized, visible both intra- and retroperitoneally (*B* and *D*, arrowheads).

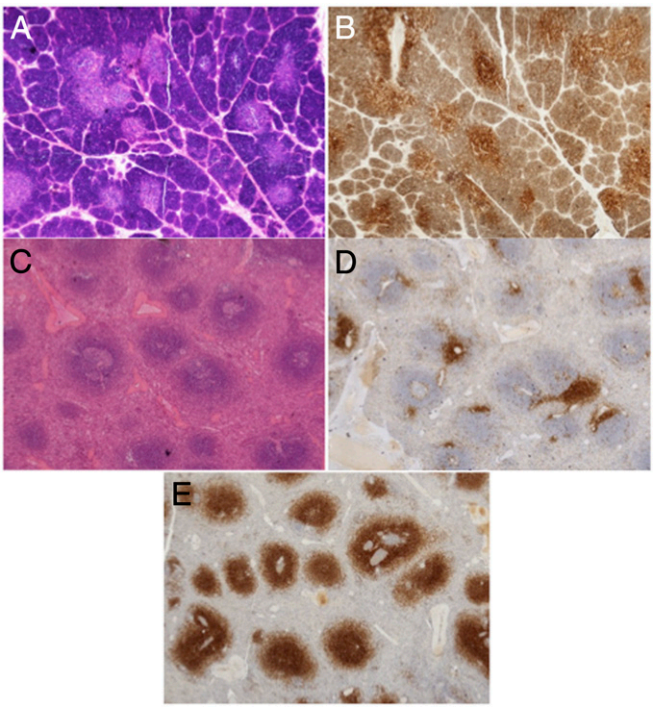

Fig. 3. Architecture of the thymus and spleen in a SCID patient (P10) 3.5 mo after HLA-identical HSCT. (*A*) A normal lobular architecture and the presence of corticomedullary differentiation in the thymus, with dense cortical areas and paler medullary areas; hematoxylin and eosin (H&E), magnification 20×. (*B*) A normal thymus T cell pattern, with more intense CD3 staining in the medullary areas, magnification 20×. (*C*) Normal architecture of the spleen, with an alternation of white pulp (containing secondary B cell follicles) and red pulp; H&E, magnification 20×. (*D*) A normal B cell pattern in the spleen, showing B cell follicles in the white pulp and a few B cells in the red pulp; anti-CD20, magnification 20×. (*E*) A normal T cell pattern, showing a T cell population around the arterioles in the white pulp; anti-CD3, magnification 20×.

germinal centers, and T cells in periarteriolar sheaths in the white pulp (Fig. 3 *C–E*). Remarkably, no Peyer patches were found anywhere in the gut (jejunum, ileum, and colon), whereas very few T and B cells were detected in the lamina propria (Fig. 4 *A–D*). In sharp contrast, the appendix (Fig. 4 *E–G*) contained well-organized lymphoid structures with T cell areas and secondary B cell follicles.

Detection of "Ectopic" Lymphoid Structures in Lung Tissue from P10 and P11. Lung tissue from P10 contained areas of organized peribronchial inflammation containing T and B cells. This suggested the development of ectopic, bronchial TLOs (Fig. 5). P11's explanted lung samples (collected at the time of his lung transplantation, 18 y after HSCT) were greatly modified, with widespread, severe bronchiectasis and alveolar pneumonitis (Fig. 6). Lymphoid follicles containing follicular dendritic cells were detected in bronchovascular areas, together with T and B cells as observed in the inflammatory lesions detected in a lung segmentectomy of control (non-SCID) patient with extensive postinfection bronchiectasis (Figs. 5 *D–F* and 6).

The Absence of LTi Cells in SCID Patients. Like the closely related ILC3, LTi cells are $CD3^-$ and $RORC^+$ (13). We looked for these cell subsets in immunologically active tissues from P10, P11, and controls. As depicted in Fig. 7 *A* and *C*, no such cells were detected, neither in the appendix nor in peribronchial lymphoid tissues of P10, whereas many were found in a control appendix (Fig. 7*B*) and control lung TLOs (Fig. 7*E*). Similarly, P11's peribronchial lymphoid follicles (Fig. 7*D*) were also devoid of

Table 2. Detection of lymph nodes by MRI

	Areas		Control	Patients
	Axillary	(L+R)	17/18	0/18
Periphery	Femoral	(L+R)	14/14	0/18
	Iliac	(L+R)	15/16	3/18
Thoracic	Paratracheal	(L+R)	7/18	1/18
	Aortopulmonary window, subcarina, hilar	(L+R)	21/36	1/36
	Coelio-mesenteric		6/8	6/9
	Interaortocaval		8/8	5/9
Abdominal	Paraaortic		8/8	5/9
	Hepatic hilar		3/8	0/8
	Paracaval		4/6	1/9
	Total		103/140	22/152

L, left; R, right. In one control the abdominal region could not be investigated.

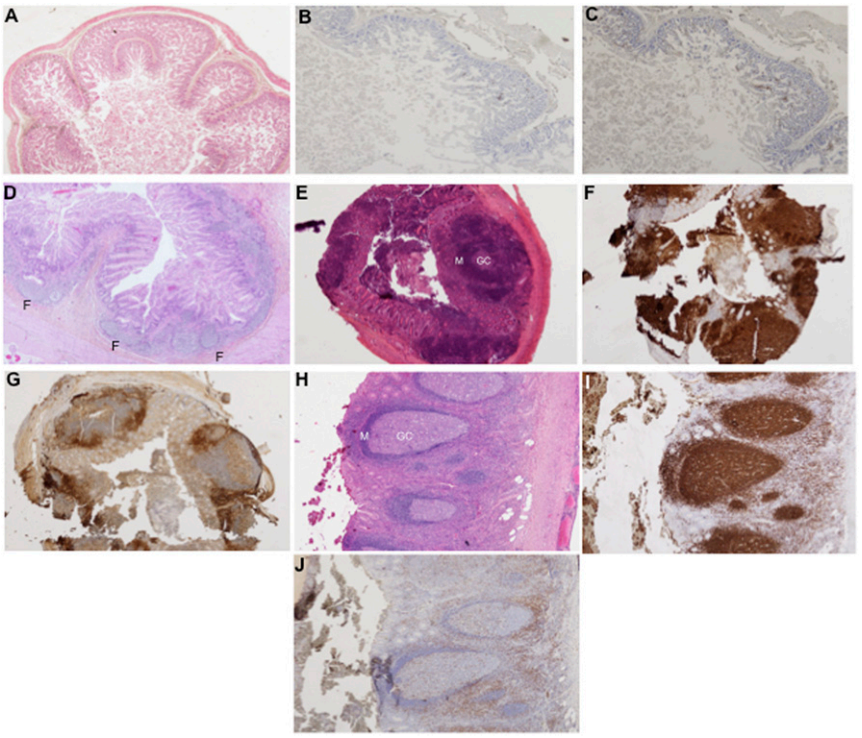

Fig. 4. Architecture of gut lymphoid structures in a SCID patient (P10). (*A*) Transversal section of the jejunum showing the normal villous architecture of the mucosa and the absence of Peyer's patches; H&E, magnification 20×. Note some autolysis due to autopsy. (*B*) Presence of very few interstitial B cells in the lamina propria of the jejunum and absence of follicles; anti-CD20, magnification 100×. (*C*) Presence of very few interstitial T cells in the lamina propria of the jejunum, anti-CD3, magnification100×. (*D*) Control jejunum showing normal villous architecture and numerous lymphoid cells within the lamina propria, including follicles (F); H&E, magnification 40×. (*E*) Transversal section of the appendix (P10), containing large B cell follicles in the lamina propria with well-defined germinal centers (GC) with mantle cell hyperplasia (M), H&E, magnification 40×. (*F*) Intense anti-CD20 staining of hyperplastic follicles; anti-CD20, magnification 40×. (*G*) Interfollicular T cell areas anti-CD3, magnification 40×. (*H*) Control appendix showing follicles with mantle (M) and prominent germinal centers (GC) in the lamina propria, magnification 40×. (*I*) Control appendix intense anti CD20 staining underlying follicles, anti-CD20, magnification 40×. (*J*) Control appendix inter follicular T cell areas and presence of a minority of intrafollicular T cells, anti-CD3, magnification 40×.

$CD3^-$ $RORC^+$ LTi and ILC3 cells. Only one such cell was detected in the lung by studying the entire slide. It is noteworthy that no $NKp46^+$ NK or ILC1 cells were found in P11 (Fig. 6). Lymphotoxin α1β2 and RANK/RANKL ligand are important lymphoid tissue-inducing molecules expressed by LTi cells (4, 29). We therefore determined whether or not they were present in the patients' lymphoid structures. Interestingly, cells in the appendix and TLOs stained positive for lymphotoxin-α and RANKL (Fig. 7 *F*–*K*).

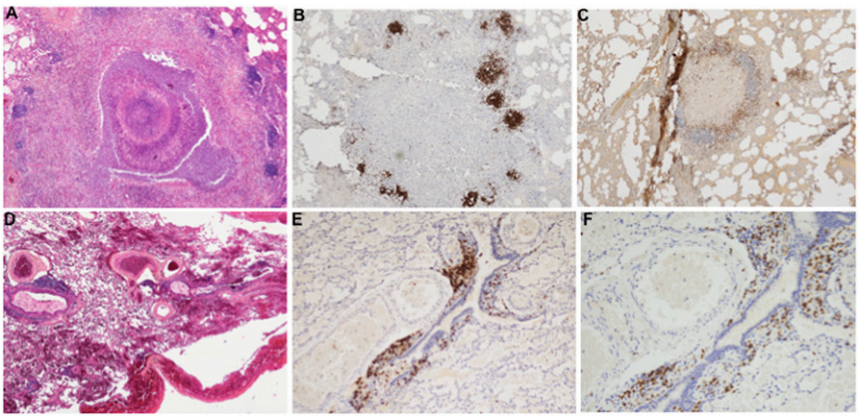

Fig. 5. Architecture of lung TLOs in P10, and a control non-SCID case with bronchiectasis. (*A*) A cross-section of a suppurative dilated bronchial structure from P10 with a fungus ball in the center and many neutrophils in the lumen and in the thick inflamed mucosa, surrounded by a large number of follicles; H&E, magnification 40×. (*B*) A large number of B cell follicles at the edge of the suppurative, organized bronchial wall; anti-CD20, magnification 40×. (*C*) Interfollicular T cells in peribronchial areas from P10 with a suppurative bronchial infection; anti-CD3, magnification 40×. (*D*) A cross-section of postinfectious bronchiectasis in a control (non-SCID) individual with bronchial lumen dilation and inflamed bronchial and peribronchial walls; H&E, magnification 40×. (*E*) Small B cell lymphoid structures in the bronchial wall of a control (non-SCID) individual with bronchiectasis; anti-CD20, magnification 100×. (*F*) Interspersed T cells within the bronchial wall in a control (non-SCID) individual with bronchiectasis; anti-CD3, magnification 100×.

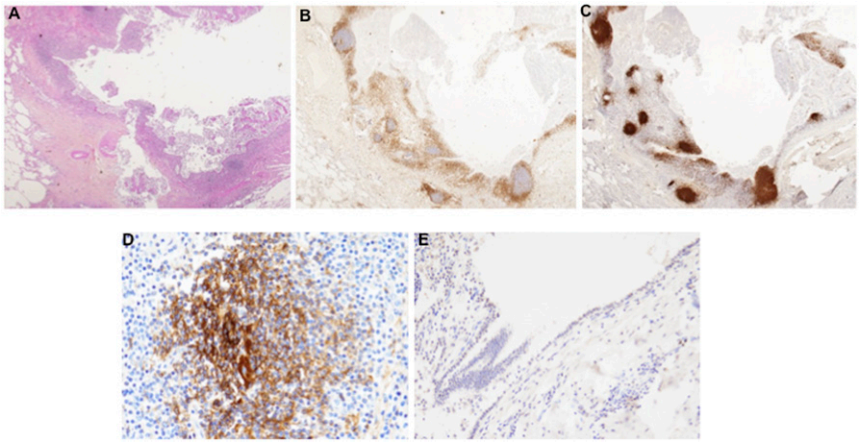

Fig. 6. Architecture of peribronchial TLOs in P11. (*A*) Inflamed bronchial wall in a suppurative dilated bronchial area; H&E, magnification 20×. (*B*) Numerous T cells in the bronchial wall; anti-CD3, magnification 20×. (*C*) Numerous lymphoid follicles in the inflamed bronchial wall; anti-CD20, magnification 20×. (*D*) Presence of a follicular dendritic meshwork within the lymphoid follicle in the inflamed bronchial wall; anti-CD21, magnification 100×. (*E*) Absence of NKP46$^+$ cells in the bronchial epithelium; anti-CD21, magnification 40×.

Discussion

This study provides insights into development of the lymphoid organs in humans. We studied SCID patients with a IL2RG (γc), JAK-3, or IL7Rα deficiencies. Given that the LTi cell ontogeny is dependent on IL7 in mice, we expected the patients to lack this cell lineage (4). Previous postmortem studies of a few nontransplanted patients have shown that peripheral lymph nodes were indeed not present. This contrasts with the presence of lymph node-like structures (albeit devoid of lymphocytes) in other SCIDs, such as RAG-1 deficiency (23). Here, we studied tissue samples and in vivo imaging data from patients who had undergone nonmyeloablative HSCT. This treatment had corrected the T cell immunodeficiency but had not led to the engraftment or differentiation of any of the other hematopoietic cell subsets (Table 1). In a postmortem examination, there was a striking absence of lymph nodes, tonsils, and Peyer patches in P10 despite definitive evidence of T cell development. The absence of lymph nodes contrasted sharply with the normal splenic architecture, including T cell periarteriolar sheath areas, the T and B cell-containing lymphoid structures in the appendix, and peribronchial TLOs. The latter were also seen in lung tissue from another transplanted SCID-X1 patient.

Ability to draw firm conclusions with regard to this unique dataset is obviously limited by the number of patients, and these circumstances are very rare. Nevertheless, the absence of tonsils and peripheral lymph nodes in the other nine transplanted IL2RG (γc)/JAK 3/IL-7Rα SCID patients with donor T cells is consistent with the pathology findings. MRI revealed how few lymph nodes were present overall. However, the presence of lymph nodes at the very same sites in our patients (i.e., celiomesenteric, interaortocaval, and paraaortic sites) suggest that the genesis of SLOs can be driven by one or more alternative mechanisms. These events thus appeared to be site-dependent. Lymph node genesis might be related to the overall organogenesis of gut-associated lymphoid tissue (GALT) since the celiomesenteric, interaortocaval, and paraaortic lymph nodes drain the gut tissue (30–32). We cannot completely rule out the generation of SLOs induced by a few residual, donor-derived LTi cells, although it is difficult to see why this would happen only in certain discrete areas of the abdomen.

Taken as a whole, these data suggest that the development of most SLOs in humans (i.e., lymph nodes and Peyer patches) is IL-7Rα/γc/JAK-3–dependent because, as observed in mice, the LTi cells are likely to depend on this pathway (4). The persistent lack of SLOs in SCID patients with post-HSCT split chimerism (i.e., donor T cells and host non-T cell leukocytes) might result from transient activity of LTi cells during fetal life only, and thus little capacity for postnatal development of SLOs. A lack of donor LTi cell differentiation is more likely, as suggested by the concomitant lack of LTi-related ILC subsets in these SCID patients (19) and RORC$^+$ CD3$^-$ cells in lymphoid-rich tissue sections from P10 and P11.

The presence of some T and B cell–containing areas within P10's spleen also fits with the LTi-independent white pulp formation observed in mice (4–7, 33). The presence of some T and B cells in the gut lamina propria is noteworthy as also observed previously in biopsies from living patients (19). These data show that the development of GALT might be at least partially independent of LTi cells and thus could occur even when the formation of Peyer's patches is impaired (34). Nevertheless, given the lack of available data, we cannot exclude that Peyer patches have developed later in life of these patients post-HSCT, as some T and B lymphocytes were detected in the lamina propria biopsy specimen obtained 1.5 to several years after HSCT (19). One of the most striking and unexpected findings concerns the presence of normal or perhaps even hyperplastic lymphoid structures in P10's appendix. A comparison with lymphoid organ development in mice is not relevant here because the species lacks an appendix. The absence of RORC$^+$ CD3$^-$ cells in P10's appendix suggests that the formation of this organ does not depend on LTi cells. This formation of lymphoid structures in the human appendix may also reflect that local immune responses have a hitherto unexpected role in controlling the microbiota at the border between bacteria-poor and bacteria-rich areas of the gut (35). Rhee et al. (36) indeed found in rabbits that the B cell repertoire shift in the appendix does not occur when the appendix is ligated and sequester from intestinal microflora.

In both P10 and P11, we clearly detected induced bronchus-associated lymphoid tissues, including organized structures with follicular dendritic cells, B cell follicles, and interfollicular T cells. These structures have also been described in immunocompetent humans in the context of infections and deleterious immune reactions (15, 37–39). They are present in LTi$^-$ mice in a context of experimental viral infection. Shikhagaie et al. (14) have shown that TLOs in the lungs of patients with chronic bronchopulmonary obstruction contain LTi-like cells usually found close to high endothelial venule cells. In contrast, TLOs in lung tissue from P10 and P11 did not contain RORC$^+$ CD3$^-$ cells. The mechanisms underlying their formation have not fully been identified. Recently, a role of the chemokine receptor CCR7 in the induction and maintenance of these structures has been reported, while two distinct routes of

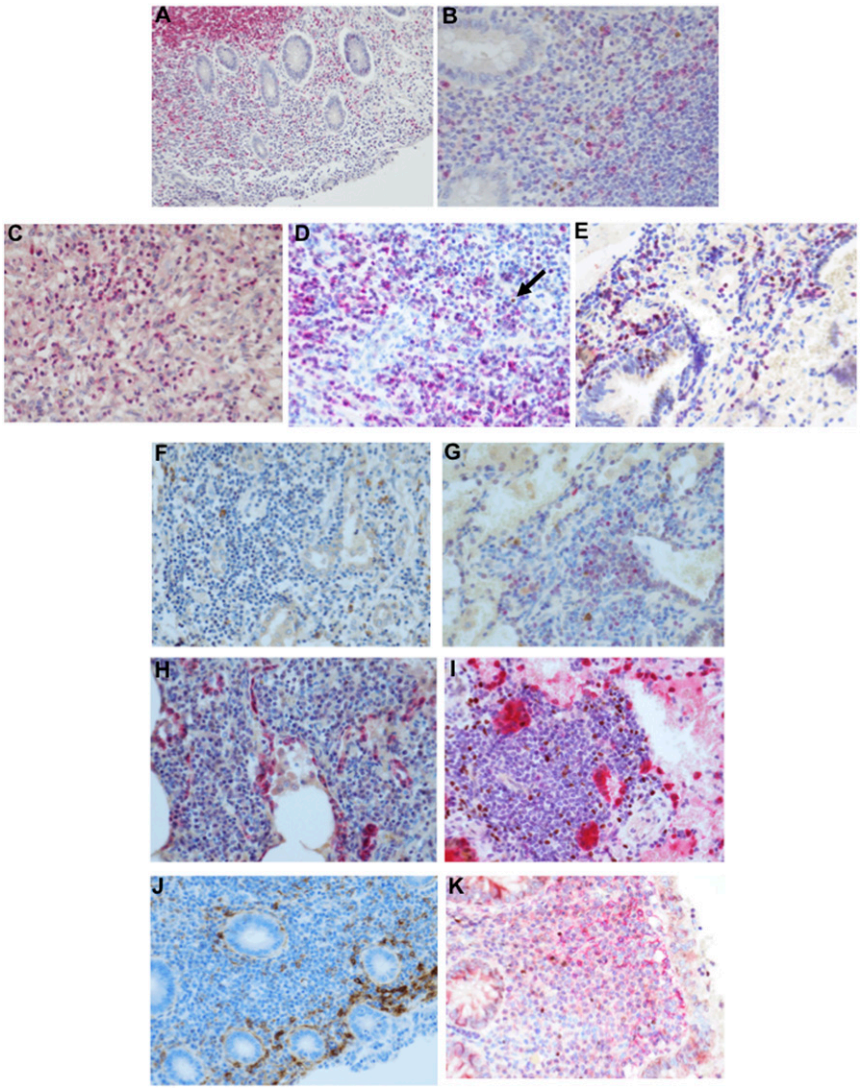

Fig. 7. Absence of RORC$^+$ CD3$^-$ cells in the appendix and peribronchial lymphoid structures in P10 and P11, and presence of LTα$^+$ and RANKL$^+$ cells. (*A*) P10's appendix: absence of RORC$^+$ CD3$^-$ cells in the lamina propria, and the presence of CD3$^+$ T cells; double staining with anti-RORC (*Brown*) and anti-CD3 (red), magnification 200×. (*B*) The control's appendix: the presence of RORC$^+$CD3$^-$ cells in the lamina propria (arrows); double staining with anti-RORC (brown), anti-CD3 (red), magnification 200×. (*C*) P10's peribronchial lymphoid structure: presence of a numerous CD3$^+$ T cells without RORC$^+$ CD3$^-$ cells; double staining with anti-RORC (brown) and anti-CD3 (red), magnification 400×. (*D*) P11's peribronchial lymphoid structure: the presence of a large number of CD3$^+$ T cells but no RORC$^+$ CD3$^-$ cells with the exception of single cell (arrow); double staining with anti-RORC (brown) and anti-CD3 (red), magnification 400×. (*E*) The control's peribronchial lymphoid structure: presence of RORC$^+$CD3$^-$ cells in the TLOs (arrows), double staining with anti-RORC (brown), anti-CD3 (red), magnification 400×. (*F*) P10's LTα$^+$ TLOs in the lung: the presence of few intracytoplasmic Ltα$^+$/RORC$^-$ cells in the peribronchial area and the absence of RORC$^+$ cells; double staining with anti-RORC (red) and anti-LTα (brown), magnification 200×. (*G*) The control's LTα$^+$ TLOs in the lung: the presence of intracytoplasmic Ltα$^+$ cells in the peribronchial area and the presence of numerous RORC$^+$ cells with red nuclear staining, double staining with anti-RORC (red), anti-LTα (brown), magnification 200×. (*H*) P10's RANKL$^+$ TLOs in the lung: the absence of RORC$^+$ cells and presence of RORC-RANKL$^+$ intracytoplasmic epithelial lining cells; double staining with anti-RORC (brown) and anti-RANKL (red), magnification 200×. (*I*) The control's RANKL$^+$ TLOs in the lung: the presence of numerous RORC$^+$ RANKL$^-$ lymphocytes and RORC$^-$ RANKL$^+$ epithelial lining cells; double staining with anti-RORC (brown) and anti-RANKL (red), magnification 200×. (*J*) P10's RANKL$^+$ structures in the appendix: the presence of RANKL$^+$ intracytoplasmic cells in the upper part of the lamina propria; anti-RANKL, magnification 200×. (*K*) The control's RANKL$^+$ structures in the appendix: the presence of RANKL$^+$ RORC$^-$ intracytoplasmic cells in the upper part of the lamina propria, and RORC$^+$ RANKL$^-$ lymphoid cells; double staining with anti-RORC (brown) and anti-RANKL (red).

homing for blood-derived lymphocytes toward TLO have been characterized (40).

Collectively, these results raise the question of how SLOs form in the appendix and other distinct abdominal areas and how lung TLOs form in the absence of LTi cells. Could the LTi cells be replaced by "LTi-like cells" that express the same key molecules required for the generation of lymphoid structures (i.e., LTα1β2, RANK, and RANKL) (4, 41)? It would be useful to characterize these putative LTi-like cells and to determine additional candidate molecules (e.g., TNF-α) (42), as several stromal cells are involved in lymphoid structures formation (43). One can speculate that signals related to the microbiota might have a postnatal role in the formation of the appendix and intraabdominal lymph nodes. Alternatively, it might be possible that appropriate stromal environments for the formation of SLO are present in the location of lymph node development. Actually, both hypotheses are not contradictory, since microflora-induced products could modulate the stromal environment (43, 44). These structures could also merely be

tertiary lymphoid structures induced by the microflora rather than bona fide SLO. It remains, however, to be known whether they could serve as niches for naïve lymphocytes.

Regardless of the exact mechanisms underlying the development of SLOs and TLOs, it is remarkable to see that γc/JAK-3/IL-7Rα–deficient patients with only donor T cells post-HSCT are able to deal with most pathogens—at least those present in the Western world—and are doing well after up to 40 y of follow-up. This is possible as long as functional B cells are present or the patients receive immunoglobulin replacement therapy (IRT). Similar findings were previously reported for NK/ILC deficiency (19) but now extend to the development of most of the SLOs. Our results emphasize the robustness of the human immune system development pathways and also indicate that even a small naïve T (B) lymphocyte reservoir can be mobilized to mount a protective immune response, probably through TLOs. Do the residual lymphoid organs in the abdomen, spleen, the gut lamina propria, the appendix, and (perhaps) the bone marrow constitute such a small cell reservoir? Despite the obvious limitations of the present study, we found that an immune system that is organized, for example, with few SLOs, as well as in the absence of NK and ILC cells, can work reasonably well in humans.

Materials and Methods

Study Design. The study aimed at identifying lymphoid structures in SCID patients with a genetic deficiency in γc, JAK3 or IL7-Rα, once transplanted. Because these patients exhibit a split chimerism with only T lymphocytes of donor origin (Table 1), it was anticipated that cells required for lymphoid organogenesis will be lacking and, thus, lymph node structure possibly deficient. The approaches consisted in in vivo analysis of lymph node structures by MRI in a cohort of such patients and healthy age-matched controls. In addition, pathology documents from a deceased patient and from explanted lungs of another SCID patient were analyzed.

Participants. We studied nine patients (P1 to P9) with SCID-X1 (γc deficiency; $n = 5$), JAK3 deficiency ($n = 3$), or IL-7 Rα deficiency ($n = 1$) and who had undergone HSCT between 1977 and 2005 without myeloablative conditioning. All were alive at the time of the study, with a median follow-up time of 29 (16 to 44) y (Table 1). Only T cells of donor origin were detected by using flow cytometry with anti HLA antibodies (45). According to the result of high-throughput sequencing, the TCR-VB CDR3 repertoire was polyclonal. Four of the patients were receiving IRT. Three patients had a chronic human papillomavirus (HPV) infection, as described previously in a cohort of transplanted patients with γc/JAK 3 SCID (46) (Table 1). This infection probably resulted from of nonhematopoietic consequences of γc JAK3/IL-7Rα deficiencies (i.e., defective keratinocytes) (46). Patients were otherwise doing well. We screened the patients for visible tonsils and palpable peripheral lymph nodes and also used 3 Tesla MRI to look for lymph nodes in the thorax and abdomen. Nine healthy, age-matched controls (five males and four females, median age 32 y [26 to 41]) were also enrolled in the MRI study.

Patient 10 was diagnosed with SCID in 1972 at the age of 7 mo; he had meningoencephalitis with pneumopathy caused by *Listeria monocytogenes*. There was a history of early death among boys in the mother's family (*SI Appendix*, Fig. S2). A diagnosis of immunodeficiency was suggested by the lack of thymic shadow on the chest X-ray, the absence of visible tonsils and palpable peripheral lymph nodes, a negative phytohemagglutinin (PHA) skin test, a defective lymphocyte proliferation response to PHA, and an absence of detectable antibodies to tetanus toxoid, polioviruses, and *Listeria*. SCID-X1 was retrospectively diagnosed after a heterozygous C318 G > A mutation, leading to a C102Y mutation in the *IL2RG* gene was found in the patient's mother and sister (*SI Appendix*, Fig. S2). He received a conditioning-free HLA A-B genoidentical HSCT from his sister. The observation of an in vitro proliferation response to PHA, a positive PHA skin test, and an XX karyotype in PHA-induced lymphoblasts suggested that the SCID had been corrected. Nevertheless, P10 died 3.5 mo post-HSCT from the sequelae of encephalitis (including intractable seizures). An extensive postmortem examination was carried out in 1972 by C. Nezelof (Necker Children's Hospital, Paris, France). An examination of the brain revealed hydrocephaly and many necrotic areas (notably in the brainstem and cerebellum) but no signs of active *Listeria* infection that had been treated with antibiotics.

Patient 11 was diagnosed with SCID at the age of 5 mo following the observation of *Pneumocystis jiroveci* pneumopathy, profound T/NK cell lymphocytopenia, defective γc expression on B cells, and a c.677 G > A, p.R226K mutation in *IL2RG*. At the age of 6 mo, the patient received a T cell–depleted haploidentical HSCT from his father, after nonmyeloablative conditioning with oral busulfan (total dose: 8 mg/kg) and intravenous cyclophosphamide (200 mg/kg). The immediate post-HSCT period was uneventful. Evidence of sustained T cell development was subsequently noted, with >1,400/μL CD4 and CD8 T cells in 2003, and an in vitro proliferation response to mitogens and antigens. The NK cell count remained very low (15/μL). Between 1989 and 2003, the patient was lost to follow-up and ceased IRT. Recurrent lung infections and severe bronchiectasis caused a rapidly progressing drop in lung capacity. The patient received a lung transplant in 2005. The patient resumed IRT and is doing well. The T cell counts remained stable. An HLA chimerism analysis of the blood showed that the T cells were of donor origin and the other leukocyte populations were of host origin. Data were collected on patients' characteristics, HSCT, immune reconstitution, chimerism, and clinical outcome.

Study Registration Approval. The study was approved by the local institutional review board (Comité de Protection des Personnes Ile de France XI, Paris, France) and registered at https://clinicaltrials.gov/ (NCT04246840). All subjects provided informed consent.

MRI Analysis. MRI was performed on a 3 Tesla system (MR750, GE Healthcare) with a 32-channel body array coil. Patients were placed in the supine position and wore an abdominal belt for respiratory gating. The thorax, abdomen, and pelvis were examined with the following sequences: axial two-dimensional (2D) T2-weighted PROPELLER, coronal 2D T2-weightedSSFSE, and axial 2D diffusion-weighted imaging (DWI) at bO and 1,000 (47, 48).

The radiologist who analyzed all the anonymized MRI data for cases and controls was blinded to each individual's clinical and laboratory data. In each individual, eight areas of the thorax and nine areas of the abdomen and pelvis were scored for the presence or absence of lymph nodes. If lymph nodes were present, the number and the greatest dimension of the major lymph node were noted. A lymph node was defined as a round or oval tissue structure with DWI hypersignal in a lymph node area.

Immunohistochemistry. Paraffin-embedded sections (thickness: 3 μm) were prepared from P10's autopsy specimens collected in 1972 and explanted lung tissue from P11 and immunohistochemically stained on a Leica Bond III automate (Leica Microsystems) using either BOND ER1 (pH 6) or ER2 (pH 9) epitope retrieval solutions (Leica Microsystems), depending on the primary antibodies. BOND Polymer Refine Detection kits (Leica Microsystems) with diaminobenzidine or Fast red (or both sequentially for serial screening) were used for detection. The sections were probed with primary antibodies against CD3 (CD3 polyclonal, A0452501, Agilent), CD20 (L26, M075501, Agilent), CD21 (2G9, CD21-2G9-L-CE), NKP46 (85EB, Innate Pharma), RORC (RORγt, 6F3.1, Merck), lymphotoxin-α (polyclonal, HPA07729, Sigma Aldrich), RANK (N2B, Amgen), and RANKL (M366, Amgen)

Data Availability. All study data are included in the article and *SI Appendix*.

ACKNOWLEDGMENTS. The authors thank Olivier Pellé and Marie-Claude Stolzenberg for technical help and Malika Tiouri for secretarial assistance. This work was funded by a grant from College de France (Chaire de Médecine Expérimentale).

1. M. F. Flajnik, A cold-blooded view of adaptive immunity. *Nat. Rev. Immunol.* **18**, 438–453 (2018).
2. D. M. Carragher, J. Rangel-Moreno, T. D. Randall, Ectopic lymphoid tissues and local immunity. *Semin. Immunol.* **20**, 26–42 (2008).
3. M. F. Vondenhoff *et al*., Separation of splenic red and white pulp occurs before birth in a LTalphabeta-independent manner. *J. Leukoc. Biol.* **84**, 152–161 (2008).
4. S. A. van de Pavert, R. E. Mebius, New insights into the development of lymphoid tissues. *Nat. Rev. Immunol.* **10**, 664–674 (2010).
5. Y. E. Bar-Ephraïm, R. E. Mebius, Innate lymphoid cells in secondary lymphoid organs. *Immunol. Rev.* **271**, 185–199 (2016).
6. R. E. Mebius, P. Rennert, I. L. Weissman, Developing lymph nodes collect CD4+CD3-LTbeta+ cells that can differentiate to APC, NK cells, and follicular cells but not T or B cells. *Immunity* **7**, 493–504 (1997).
7. D. L. Drayton, S. Liao, R. H. Mounzer, N. H. Ruddle, Lymphoid organ development: From ontogeny to neogenesis. *Nat. Immunol.* **7**, 344–353 (2006).
8. A. T. Krishnamurty, S. J. Turley, Lymph node stromal cells: Cartographers of the immune system. *Nat. Immunol.* **21**, 369–380 (2020).
9. H. Yoshida *et al*., Different cytokines induce surface lymphotoxin-alphabeta on IL-7 receptor-alpha cells that differentially engender lymph nodes and Peyer's patches. *Immunity* **17**, 823–833 (2002).

10. X. Cao *et al*., Defective lymphoid development in mice lacking expression of the common cytokine receptor gamma chain. *Immunity* **2**, 223–238 (1995).
11. S. Y. Park *et al*., Developmental defects of lymphoid cells in Jak3 kinase-deficient mice. *Immunity* **3**, 771–782 (1995).
12. S. Adachi, R. A. Gottlieb, B. M. Babior, Lack of release of cytochrome C from mitochondria into cytosol early in the course of Fas-mediated apoptosis of Jurkat cells. *J. Biol. Chem.* **273**, 19892–19894 (1998).
13. T. Cupedo *et al*., Human fetal lymphoid tissue-inducer cells are interleukin 17-producing precursors to RORC+ CD127+ natural killer-like cells. *Nat. Immunol.* **10**, 66–74 (2009).
14. M. M. Shikhagaie *et al*., Neuropilin-1 is expressed on lymphoid tissue residing lti-like group 3 innate lymphoid cells and associated with ectopic lymphoid aggregates. *Cell Rep.* **18**, 1761–1773 (2017).
15. S. J. Gould, P. G. Isaacson, Bronchus-associated lymphoid tissue (BALT) in human fetal and infant lung. *J. Pathol.* **169**, 229–234 (1993).
16. C. Pitzalis, G. W. Jones, M. Bombardieri, S. A. Jones, Ectopic lymphoid-like structures in infection, cancer and autoimmunity. *Nat. Rev. Immunol.* **14**, 447–462 (2014).
17. R. Spolski, P. Li, W. J. Leonard, Biology and regulation of IL-2: From molecular mechanisms to human therapy. *Nat. Rev. Immunol.* **18**, 648–659 (2018).
18. A. Fischer *et al*., Severe combined immunodeficiency. A model disease for molecular immunology and therapy. *Immunol. Rev.* **203**, 98–109 (2005).
19. F. Vély *et al*., Evidence of innate lymphoid cell redundancy in humans. *Nat. Immunol.* **17**, 1291–1299 (2016).
20. H. Spits *et al*., Innate lymphoid cells—A proposal for uniform nomenclature. *Nat. Rev. Immunol.* **13**, 145–149 (2013).
21. I. E. Ishizuka *et al*., Single-cell analysis defines the divergence between the innate lymphoid cell lineage and lymphoid tissue-inducer cell lineage. *Nat. Immunol.* **17**, 269–276 (2016).
22. E. Vivier *et al*., Innate lymphoid cells: 10 years on. *Cell* **174**, 1054–1066 (2018).
23. F. Facchetti, L. Blanzuoli, M. Ungari, O. Alebardi, W. Vermi, Lymph node pathology in primary combined immunodeficiency diseases. *Springer Semin. Immunopathol.* **19**, 459–478 (1998).
24. R. H. Buckley *et al*., Hematopoietic stem-cell transplantation for the treatment of severe combined immunodeficiency. *N. Engl. J. Med.* **340**, 508–516 (1999).
25. S. Y. Pai *et al*., Transplantation outcomes for severe combined immunodeficiency, 2000-2009. *N. Engl. J. Med.* **371**, 434–446 (2014).
26. B. Neven *et al*., Long-term outcome after hematopoietic stem cell transplantation of a single-center cohort of 90 patients with severe combined immunodeficiency. *Blood* **113**, 4114–4124 (2009).
27. R. H. Buckley, Transplantation of hematopoietic stem cells in human severe combined immunodeficiency: Longterm outcomes. *Immunol. Res.* **49**, 25–43 (2011).
28. L. P. Hale, R. H. Buckley, J. M. Puck, D. D. Patel, Abnormal development of thymic dendritic and epithelial cells in human X-linked severe combined immunodeficiency. *Clin. Immunol.* **110**, 63–70 (2004).
29. M. B. Alimzhanov *et al*., Abnormal development of secondary lymphoid tissues in lymphotoxin beta-deficient mice. *Proc. Natl. Acad. Sci. U.S.A.* **94**, 9302–9307 (1997).
30. S. A. Houston *et al*., The lymph nodes draining the small intestine and colon are anatomically separate and immunologically distinct. *Mucosal Immunol.* **9**, 468–478 (2016).
31. S. A. Matalon *et al*., Anorectal cancer: Critical anatomic and staging distinctions that affect use of radiation therapy. *Radiographics* **35**, 2090–2107 (2015).
32. D. Esterházy *et al*., Compartmentalized gut lymph node drainage dictates adaptive immune responses. *Nature* **569**, 126–130 (2019).
33. S. M. Lewis, A. Williams, S. C. Eisenbarth, Structure and function of the immune system in the spleen. *Sci. Immunol.* **4**, eaau6085 (2019).
34. T. D. Randall, R. E. Mebius, The development and function of mucosal lymphoid tissues: A balancing act with micro-organisms. *Mucosal Immunol.* **7**, 455–466 (2014).
35. M. J. H. Girard-Madoux *et al*., The immunological functions of the appendix: An example of redundancy? *Semin. Immunol.* **36**, 31–44 (2018).
36. K. J. Rhee *et al*., Positive selection of the peripheral B cell repertoire in gut-associated lymphoid tissues. *J. Exp. Med.* **201**, 55–62 (2005).
37. J. E. Moyron-Quiroz *et al*., Role of inducible bronchus associated lymphoid tissue (iBALT) in respiratory immunity. *Nat. Med.* **10**, 927–934 (2004).
38. K. Neyt, F. Perros, C. H. GeurtsvanKessel, H. Hammad, B. N. Lambrecht, Tertiary lymphoid organs in infection and autoimmunity. *Trends Immunol.* **33**, 297–305 (2012).
39. A. Silva-Sanchez, T. D. Randall, Role of iBALT in respiratory immunity. *Curr. Top. Microbiol. Immunol.* **426**, 21–43 (2020).
40. H. Fleige *et al*., Manifold roles of CCR7 and its ligands in the induction and maintenance of bronchus-associated lymphoid tissue. *Cell Rep.* **23**, 783–795 (2018).
41. P. De Togni *et al*., Abnormal development of peripheral lymphoid organs in mice deficient in lymphotoxin. *Science* **264**, 703–707 (1994).
42. G. C. Furtado *et al*., TNFα-dependent development of lymphoid tissue in the absence of RORγt$^+$ lymphoid tissue inducer cells. *Mucosal Immunol.* **7**, 602–614 (2014).
43. J. J. Koning, R. E. Mebius, Stromal cells and immune cells involved in formation of lymph nodes and their niches. *Curr. Opin. Immunol.* **64**, 20–25 (2020).
44. C. Gago da Graça, L. G. M. van Baarsen, R. E. Mebius, Tertiary lymphoid structures: Diversity in their development, composition, and role. *J. Immunol.* **206**, 273–281 (2021).
45. M. Schumm *et al*., Flow cytometry with anti HLA-antibodies: A simple but highly sensitive method for monitoring chimerism and minimal residual disease after HLA-mismatched stem cell transplantation. *Bone Marrow Transplant.* **39**, 767–773 (2007).
46. C. Laffort *et al*., Severe cutaneous papillomavirus disease after haemopoietic stem-cell transplantation in patients with severe combined immune deficiency caused by common gammac cytokine receptor subunit or JAK-3 deficiency. *Lancet* **363**, 2051–2054 (2004).
47. N. Mir, S. A. Sohaib, D. Collins, D. M. Koh, Fusion of high b-value diffusion-weighted and T2-weighted MR images improves identification of lymph nodes in the pelvis. *J. Med. Imaging Radiat. Oncol.* **54**, 358–364 (2010).
48. S. Ganeshalingam, D. M. Koh, Nodal staging. *Cancer Imaging* **9**, 104–111 (2009).